Mixed Matrix Membranes Based on 6FDA Polyimide with Silica and Zeolite Microsphere Dispersed Phases

Beatriz Zornoza, Carlos Téllez, and Joaquín Coronas
Chemical and Environmental Engineering Dept. and Instituto de Nanociencia de Aragón (INA), Universidad de Zaragoza, 50018 Zaragoza, Spain

Omoyemen Esekhile and William J. Koros
School of Chemical and Biomolecular Engineering, Georgia Institute of Technology, 311 Ferst Drive, Atlanta, GA 30332, United States

DOI 10.1002/aic.15011
Published online August 25, 2015 in Wiley Online Library (wileyonlinelibrary.com)

Mixed matrix membranes (MMMs) prepared with 6FDA-DAM polymer using ordered mesoporous silica MCM-41 spheres (MSSs), Grignard surface functionalized MSSs (Mg-MSSs) and hollow zeolite spheres are studied to evaluate the effects of surface modification on performance. Performance near or above the so-called permeability-selectivity trade-off curve was achieved for the H_2/CH_4, CO_2/N_2, CO_2/CH_4, and O_2/N_2 systems. Two loadings (8 wt % and 16 wt %) of MSSs were tested using both constant volume and Wicke–Kallenbach sweep gas permeation systems. Besides single gas H_2, CO_2, O_2, N_2, and CH_4 tests, mixed gas (50/50 vol %) selectivities were obtained for H_2/CH_4, CO_2/N_2, CO_2/CH_4, and O_2/N_2 and found to show enhancements vs. single gases for CO_2 including cases. Mg-MSS/6FDA-DAM was the best performing MMM with H_2/CH_4, CO_2/N_2, CO_2/CH_4, and O_2/N_2 separation selectivities of 21.8 (794 Barrer of H_2), 24.4 (1214 Barrer of CO_2), 31.5 (1245 Barrer of CO_2), and 4.3 (178 Barrer of O_2), respectively. *AIChE J*, 61: 4481–4490, 2015
Keywords: mixed matrix membrane, gas separation, polyimide 6FDA-DAM, ordered mesoporous silica, zeolite microspheres, surface modification

Introduction

Identification of an appropriate polymer matrix and suitable dispersed filler phase influence successful formation of mixed matrix membranes (MMMs)[1] able to overcome the so-called Robeson upper bound trade-off curve for permeability and selectivity.[2,3] Resistance to plasticization is required for many gas separation processes[4,5] and functionalized fillers are attractive to achieve high performance with adequate plasticization resistance.[6]

An aromatic polyimide, 6FDA-DAM used in this work has good thermal and chemical stabilities with attractive transport properties and processability in common solvents.[7–12] The 6FDA-DAM shows better intrinsic performance for many gas separations vs. polysulfone or polyimide Matrimid®, so it was a good choice for the current work.[13]

Different fillers have been incorporated into polymer matrices, including ordered mesoporous silica,[14–18] nonporous silica,[5,19] carbon molecular sieves,[20] carbon nanotubes,[21] zeolites,[22–24] and metal-organic frameworks.[25] Several reviews have considered performance of MMMs.[1,6,26–29] These reviews highlight the importance of engineering the contact between the organic and inorganic phases, since nonideal contact leads to undesirable MMM morphology and non-selective defects, which compromise the performance of the membrane.[30,31]

In this work ordered mesoporous silica MCM-41 spheres (MSSs) were used as one of the fillers to improve the already attractive intrinsic properties of the 6FDA-DAM polymer. Mesoporous materials possess sufficiently large pores (20–500 Å), which may allow penetration of polymer chains, thereby improving surface contact and dispersion. Since the discovery of the M41S family of mesoporous molecular sieves by Kresge et al.[32] these materials have received intensive research as catalysts, adsorbents, and membranes. Addition of silica particles to a polymer matrix may disrupt the polymer chain packing, leading to enhanced gas permeability.[18] Reid et al.[14] studied the influence of MCM-41 as additives in polysulfone matrices showing enhanced permeability behavior due to the large pore size of the filler, but with no change of selectivity.

Various functionalization have been explored to improve surface contact in MMM application,[16,23,33,34] Grignard treatment, developed by Shu and Husain,[23,34] was particularly useful for polyimides due to the formation of $Mg(OH)_2$ nanostructures.[24] We expected that a Grignard modification of MSS particles may also be effective on the MSSs surface.[17]

Moreover, using a MSSs starting material, a layer-by-layer surface procedure has been shown to produce hollow zeolite spheres (HZSs), with a silicalite-1 shell intergrown around a

Additional Supporting Information may be found in the online version of this article.

Correspondence concerning this article should be addressed to Beatriz Zornoza at bzornoza@unizar.es.

hollow interior.[35] Herein, we study the addition of MSSs, Mg-MSSs, and HZSs fillers within the polymer 6FDA-DAM to form MMMs. The high performance 6FDA-DAM pure polymer was characterized for sorption and plasticization and to assess the effects of thermal annealing. Permeation tests of MSSs/6FDA-DAM MMMs using both constant volume and Wicke–Kallenbach sweep gas permeation setups are discussed. Results for single gases (H_2, CO_2, O_2, N_2, and CH_4) as well as for binary gas mixtures (H_2/CH_4, CO_2/N_2, CO_2/CH_4, and O_2/N_2) are reported.

Experimental Section

Materials

Ordered mesoporous silica spheres (MSSs) were synthesized following experimental procedure described by Schulz-Ekloff et al.,[36] with modifications to the synthesis gel by Navascues et al.[37] Sodium metasilicate, Na_2SiO_3, Sigma-Aldrich, was used with cetyltrimethylammonium bromide surfactant, $C_{19}H_{42}NBr$, Sigma-Aldrich, to achieve a mesoporous structure with an initiator to enable colloidal aggregates formation (ethylacetate, $CH_3COOC_2H_5$, Sigma-Aldrich). The molar composition was: 1.5 Na_2SiO_3: 1 CTABr: 361 H_2O: 7.4 $CH_3COOC_2H_5$. The resulting whitish sol dispersion, reflecting silica condensation, was kept in a closed polypropylene flask at room temperature for 5 h and then allowed to proceed at 90°C for 50 h in the same open flask, without stirring. The final product was washed several times in distilled water and ethanol, and then filtered. The structure-directing agent was removed and the mesoporous MSSs were created by calcining at 600°C for 8 h using heating and cooling rates of 0.5°C/min.

MSSs were functionalized following the Grignard treatment (Mg-MSS) to modify the surface chemistry of the sieves, reducing the interaction solvent-sieve, and improving adherence to the polymer. The procedure contains: (1) crystal seeding, and (2) crystal growth by Grignard quenching and sonication processes, as extensively described in the literature.[23] However, for silicalite-1 (zeolite with the MFI-type structure but without Al content) the process was proved to be ineffective due to the lack of appropriate crystal seed, on which $Mg(OH)_2$ nanostructures can grow.[38] Then, a previous dispersion step of 0.5 g of MSSs in a solution of NaCl 3 M was applied to produce adequate ionic exchange. In the second step, the recovered MSS particles by filtration were placed in a reaction flask containing a magnetic stir bar. The particles and the glassware were dried at 150°C overnight in a vacuum oven. Then, 8 mL of toluene and 1.5 mL of methylmagnesium bromide, CH_3MgBr (3.0 M solution in diethylether, Sigma-Aldrich) were added into the sealed flask. The suspension was sonicated for 4 h and stirred during 12 h more under nitrogen before isopropanol was added drop by drop. To remove the residual solvents the resulting sol dispersion was centrifuged twice with isopropanol and then subjected to a series of sonication and centrifugation treatments (three 30 s periods of horn sonication with 2 min of repose and centrifugation upon dispersion with distilled water at 7000 rpm for 10 min) several times until the conductivity of the supernatant dropped below 30 μS/m. The final collected particles were dried overnight at 80°C.

As described earlier, HZSs were created using silicalite-1 seeds, of approximately 100 nm in size. The seed crystals were synthesized using a sol with the molar composition of 9 TPAOH: 25 SiO_2: 408 H_2O: 100 EtOH[13] which was autoclaved for 20 h at 100°C. To improve electrostatic interaction between the spheres and the seeds, an aqueous 0.5 M NaCl solution containing 2 mg of poly (diallyl di-methyl ammonium chloride) was added to the dispersed MSSs, followed by washing and centrifuging. The resulting suspension was placed in contact with dilute NH_4OH (pH = 9.5), and 0.25 wt % silicalite-1 seeds. Excess silicalite-1 seeds were removed by washing and a layer-by-layer seeding procedure was used to produce silicalite-1 monolayer coated in MSSs. Finally, silicalite-1 seeded MSSs were subjected to hydrothermal synthesis at 175°C for 12 h with the following molar composition: KOH: TPABr: 8 SiO_2: 2130 H_2O [40] to convert the silica to zeolite silicalite-1.

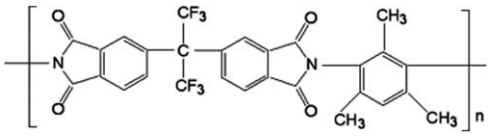

Figure 1. Chemical structure of the 6FDA-DAM polyimide.

The polymer used in this work to prepare the MMMs was 6FDA-DAM (T_g = 325°C, FFV = 0.19, density = 1.35 g/cm^3, see Figure 1), which was synthesized as reported elsewhere.[39] The monomers 6FDA (2,2-bis (3,4-carboxyphenyl) hexafluoropropane dianhydride, Sigma) and DAM (diaminomesitylene, Sigma) were purified by sublimation and polymerized to give a Mw of 81,000, as described in previous work,[24] and used to form membranes.

Preparation of 6FDA-DAM-based MMMs

MMMs with MSSs, Mg-MSSs and HZSs in 6FDA-DAM were fabricated at 8 wt % and 16 wt % to study the effect of the filler loading. A 13% polymer dope was prepared with dried 6FDA-DAM and tetrahydrofuran (THF) as solvent and rolled on a mixer overnight to get a well dispersed solution. For polymer membranes, the dope was ready for the casting; however MMMs required the following further steps: (1) drying inorganic fillers at 180°C overnight, (2) dispersing the dried particles in an ultrasonic bath for 30 min with enough THF to achieve a nonagglomerated dispersion, (3) adding 10% of the above mentioned dope for "priming" to produce low polymer/filler ratio in the solvent, (4) rolling and horn sonicating to achieve a well dispersed mixture, (5) adding the remaining 90% of the calculated dope, and (6) rolling in the mixer overnight.

The final solution was poured onto a glass flat plate (placed in a glove bag pre-saturated with THF during 3 h) and a draw knife with appropriate clearance was used to achieve the desired thickness (40 ± 10 μm). The dense membrane was formed by controlled solvent evaporation rate overnight, followed by thermal (180°C or 270°C) and vacuum treatment for 24 h with slow heating/cooling rates to remove the remaining solvent.

Characterization of fillers and membranes

MSSs, Mg-MSSs, HZSs, and the corresponding MMMs, were characterized by *scanning electron microscope* (*SEM*, JEOL JSM 6400, Jeol Corp., operating at 20 kV) coupled with an *energy-dispersive x-ray spectroscopy* (*EDX*). Polymer and MMMs cross-section were prepared by freeze-fracturing after immersion in liquid N_2. *Transmission electron microscope* (*TEM*) samples were embedded in Epofix^{TM} cold-setting resin

(Electron Microscopy Sciences) with 15/2 volume parts of embedding resin/hardener and cured for 8 h at room temperature. The resultant pieces were cut at 30–60 nm thickness using a RMC MT-XL ultramicrotome (RMC Products) with a Standard Ultraknife 45°, 3 mm diamond blade (Drukker Ultramicrotome knife, Elementsix™). The sliced sections were stained in aqueous solution, placed on carbon copper grids and subsequently observed at 200 kV in a JEOL-2000 FXII TEM (Jeol Corp.).

Powder and membranes were characterized by *x-ray diffraction* (*XRD*) using a D-Max Rigaku diffractometer with a copper anode and a graphite monochromator to select Cu-K_α radiation ($\lambda = 1.5418$ Å). Data were measured from $2\theta = 2.5°$ to 40° in steps of 0.03° and $t = 1$ s/step. *Low angle x-ray diffraction* (*LA-XRD*) spectra of the fillers were recorded on a Philips X'Pert diffractometer (PANalytical B. V.) with Bragg–Brentano geometry and Cu-Kα radiation. In this case, 2θ was recorded from 0.6° to 8°. *N_2 adsorption-desorption isotherms and BET* specific surface areas of the fillers were measured at 77 K using a porosity analyzer (TriStar 3000, Micromeritics Instrument Corp.) after outgassing at 350°C for 8 h. The pore size distributions were calculated using the Barrett–Joyner–Halenda model from the adsorption branches. *Thermogravimetric analyses* (*TGA*) were performed using a Mettler Toledo TGA/STDA 851^e. Samples of 10 mg were placed in 70 μL alumina pans and heated in air flow up to 850°C at 10°C/min maintaining the final temperature for 1 h.

High pressure sorption and permeability measurements of membranes

Sorption measurements of 6FDA-DAM-based membranes were performed up to 150 kPa using a pressure decay method described in detail elsewhere.[40]

Permeation through a polymer is described by the solution-diffusion theory, where gases dissolve into the surface of the membrane at the high-pressure feed side, then diffuse through the polymer matrix because of a concentration gradient, and finally desorb at the low pressure permeate side. Two basic parameters are typically characterized: permeability and selectivity. *Permeability* (P_i) for component i, is defined as the penetrant flux, normalized by the thickness, l, and the partial pressure drop across the membrane, Δp_i (Eq. 1)

$$P_i = \frac{\text{Flux}_i \cdot l}{\Delta p_i} \tag{1}$$

P is usually given in Barrer unit (1 Barrer = 10^{-10} $cm^3(STP)\cdot cm\ cm^{-2}\ s^{-1}\ cmHg^{-1}$). When the ideal permeabilities of each species are known in the material Eq. 2 for *ideal selectivity* or *permselectivity* ($\alpha_{i/j}$) is used. $\alpha_{i/j}$ for preferential permeating component i over component j is defined as the permeability ratio of the pure gases: i and j

$$\alpha_{i/j}(\text{ideal}) = P_i/P_j \tag{2}$$

In the case of mixed gas feeds where there may be competitive interactions between the permeating gases and the polymer, the *real selectivity* or *separation factor* is considered. In this case $\alpha_{i/j}$ expresses the relative enrichment in the permeate stream with respect to the feed composition when a gas mixture is fed to the membrane system. The separation factor is calculated in Eq. 3, being y and x the mole fraction of gas/vapor in permeate and feed sides of the membrane, respectively

$$\alpha_{i/j}(\text{real}) = \frac{y_i/y_j}{x_i/x_j} \tag{3}$$

Pure and mixed-gas permeabilites for bare 6FDA-DAM polymer and MMMs were measured using two experimental procedures. The first method was a constant volume method for single gas permeation tests, described in detail elsewhere.[41] The second method was a sweep (Wicke–Kallenbach) method[42] for single gas or multicomponent gas mixtures to determine for H_2/CH_4, CO_2/N_2, CO_2/CH_4, and O_2/N_2 binary mixtures.

The same membranes were measured using the two setups under the same standard conditions for reproducibility purposes. For the constant volume method individual gases were fed at 35°C and ~200 kPa with a downstream at vacuum. In the Wicke–Kallenbach method, both single and 50% binary mixtures were analyzed in a GC setup described elsewhere.[17] The feed enters into the membrane module placed in an oven at 35°C (at 50 cm^3(STP)/min) at pressure of ~300 kPa, with the permeate side at atmospheric pressure, which is swept with Ar (1 cm^3(STP)/min, for H_2/CH_4 mixture) or He (5 cm^3(STP)/min, for O_2/N_2, CO_2/CH_4, and CO_2/N_2 mixtures). Stream compositions were analyzed by an on-line gas microchromatograph (Agilent 3000A) equipped with TCD. In both type of setups permeabilities were obtained once the steady state of the exit stream (permeate) was reached and the separation selectivities were calculated as the ratio of experimental permeabilities. In the case of the constant volume method the steady-state permeation flux is obtained from the gradient of pressure-time response while for Wicke–Kallenbach method once the exit stream of the membrane was stabilized, typically with times longer than 3 h. Each type of membrane was fabricated and measured multiple times to provide reliable error estimates.

Results and Discussion

Characterization of fillers and MMMs

Figure 2 shows SEM/TEM images of the three fillers considered in this work: MSSs, Mg-MSSs, and HZSs, and their corresponding MMMs based on 6FDA-DAM polymer.

Images 2a,b and 2d,e, corresponding to MSSs and Mg-MSSs-based membranes, respectively, do not clearly show the $Mg(OH)_2$ nanostructures but a certain roughness of the surface of the spheres. The TEM technique, however, revealed individual particles with good contact without voids for MSS/6FDA-DAM MMM (Figure 2c). Excellent adhesion for a single Mg-MSS particle was observed in Figure 2f, where its external whisker-like structure promoted interfacial filler-polymer contact once embedded in the 6FDA-DAM polymer matrix. In addition, by EDX it was possible to analyze the Grignard treated sample obtaining an atomic percent of 6% for Mg (being the others oxygen and silicon: 72% and 22%, respectively). The calcined MSS, with nonsurface modification, showed an atomic percent of about 75% for oxygen and 25% for silicon. In both cases, the percent was calculated without accounting for the carbon, coming also from the 15 nm coating needed for EDX. By thermogravimetric analysis the weight loss of calcined MSSs (4.9%) and Mg-MSSs (18.4%) were obtained (see Figure S1 in the Supporting Information). The difference among these values, 13.5 wt %, is related to the magnesium oxide layer created in the MSSs surface, being in a similar range as that obtained by Husain et al.[43] by applying the Grignard treatment to zeolite SSZ-13.

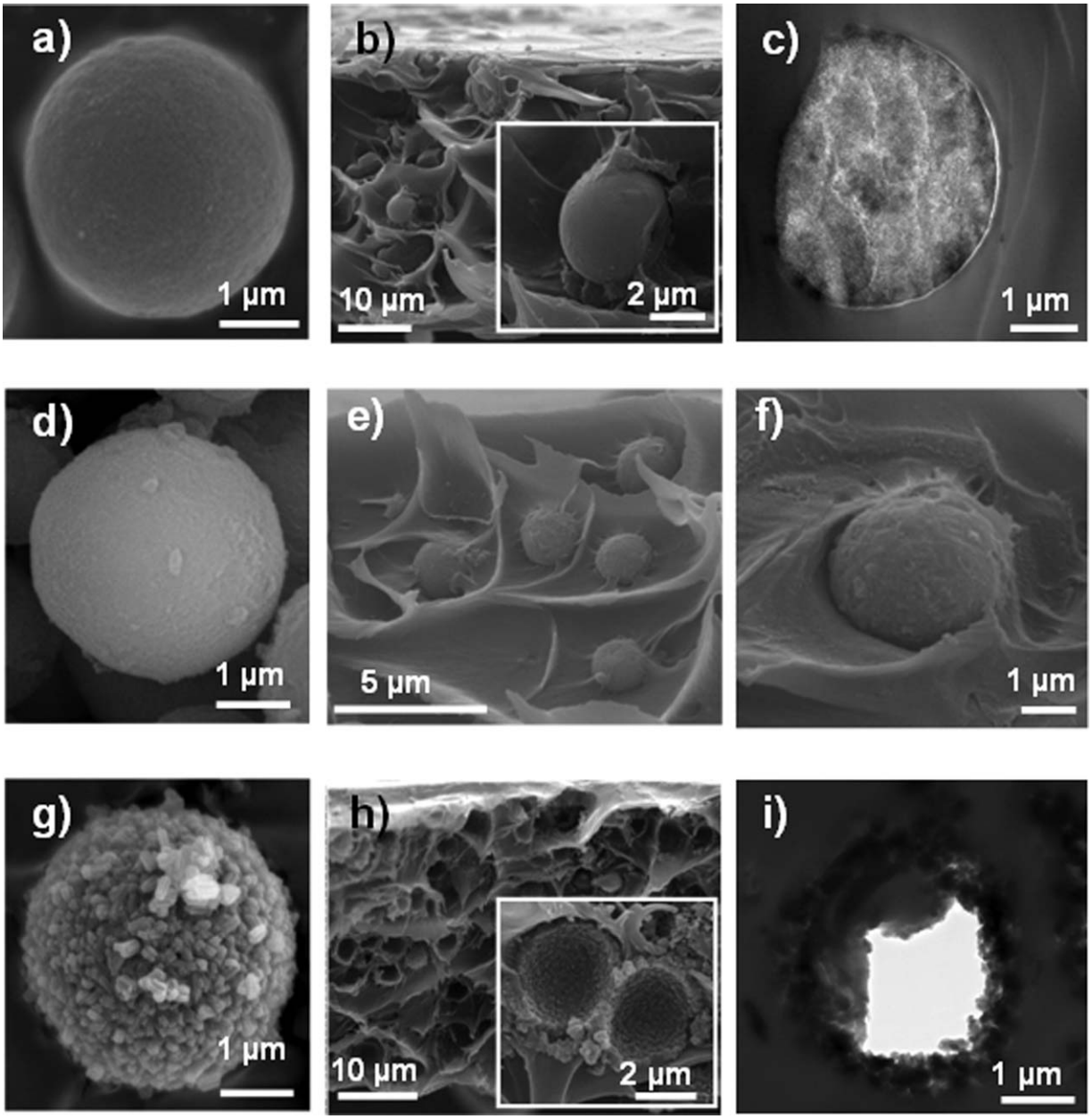

Figure 2. SEM images based of: (a–c) MSSs [(a) individual particle, (b) 8 wt % MSS/6FDA:DAM MMM, and (c) TEM image of an embedded particle], (d–f) Mg-MSSs [(d) individual particle, (e) 8 wt % Mg-MSS/6FDA-DAM MMM, and (f) inset of (e)], and (g–i) HZSs [(g) individual particle, (h) 8 wt % HZS/6FDA-DAM MMM, and (i) TEM image of an embedded particle].

The second type of filler prepared from the ordered mesoporous silica MCM-41 type structure, MSSs, was the HZSs (Figure 2g). This self-bonded molecular sieve structure prepared by the layer-by-layer (LbL) procedure, followed by hydrothermal crystallization, produced engineered particle surfaces based on silicalite-1.[37] SEM and TEM analysis of more than 30 samples showed sphere diameters of 3.1 ± 0.6 μm for MSSs, which converted into HZSs of 4.3 ± 0.7 μm during the hydrothermal synthesis. An 8 wt % filler loading showed good distribution of HZSs throughout the membrane (Figure 2h) and individual HZS particles checked by TEM (Figure 2i) show an interpenetrated zeolite-polymer composite with good interaction. The good interaction is promoted by: (1) the hydrophobic silicalite-1 surface, and (2) small silicalite-1 surface crystals of about 200 nm in size. Similar features were noted for this filler embedded in PSF Udel® and PI Matrimid® MMMs.[35]

The N_2 adsorption-desorption isotherms of the MSSs and Mg-MSSs in Figure 3 show type IV characteristic of mesoporous material, while the isotherms of HZSs show a combination of types I and IV. While MSSs show a bimodal pore structure with pores of 2.7 nm and 9 nm attributed to mesoporous and non-mesoporous MCM-41 phases, respectively (see Figure 3 inset), Mg-MSSs presented just a broad band from 2 nm to 10 nm indicating loss of porous narrow distribution, but not pore blocking. The specific adsorption isotherm for MSSs shows a BET area of 1023 ± 9 m^2/g, whereas Mg-MSSs gave a specific area of 696 ± 2 m^2/g. For the HZSs, the bimodal pore size distribution is lost, with only a small broad distribution related to the nano-silicalite-1 with specific BET

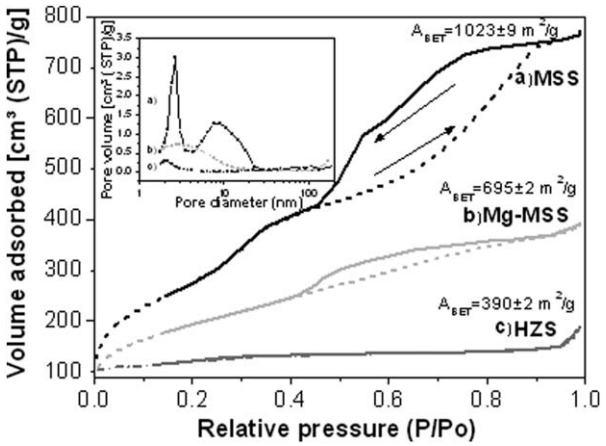

Figure 3. Adsorption (dotted lines) and desorption (solid lines) N2 isotherm branches for: (a) MSSs, (b) Mg-MSSs, and (c) HZSs.

In the inset pore BJH size distribution of the three fillers is plotted.

area and external surface of 390 ± 2 m^2/g and 108 ± 10 m^2/g, respectively.

LA-XRD and x-ray diffraction (XRD) on the three fillers (Figure 4) show a broad peak in the 15–30° range for the MSSs and Mg-MSSs, with a maximum around 23° corresponding to the amorphous band of silica. For the Mg-MSSs sample, a new peak appears at 34°, which could be related to the Mg hydroxides used in the modification of the MSSs by the Grignard method. In fact, Bae et al.[38] did not found distinguishable peaks from $Mg(OH)_2$ when applying the Grignard treatment to pure silica MFI particles except a broad peak at 38°. This can be due to the relatively low amount of $Mg(OH)_2$ with low crystallinity because of small particle size.

The LA-XRD for MSSs and Mg-MSSs in Figure 5 show a strong peak at 2.4° and a weak peak at higher 2θ angles corresponded to the planes (100) and (110). These results suggest that the MSSs (Figure 4a) have hexagonal pores typical of MCM-41[44] with the first (100) peak at $2\theta = 2.4°$ typical of $d_{100} = 3.7$ nm, based on Bragg's law. Moreover, the low angle Mg-MSSs results (Figure 4b) suggest the ordered MCM-41 structure disappears during the Grignard treatment, leading to a disordered material, consistent with the previous N_2 adsorption results. Conversely the HZSs gave the characteristic zeolite silicalite-1 spectra.

Figure 5 shows the diffractograms of the hybrid membranes prepared with MSSs, Mg-MSSs, and HZSs. The spacing of the polymer chains for the pure 6FDA-DAM membrane and the 8 wt % MSS/6FDA-DAM MMM were 5.6 and 5.5 Å, respectively. Previous studies also indicated a slight reduction in characteristic spacing due to addition of 16 wt % of ordered mesoporous silica particles.[18] Nevertheless, Figure 5 reveals a shift to higher 2·theta angles for 8 wt % Mg-MSS/6FDA-DAM (6.1 Å) and 8 wt % HZS/6FDA-DAM (6.3 Å) MMMs, indicating that the whisker-like structure of $Mg(OH)_2$ and the silicalite-1 crystals may favorably promote adhesion in a MMM.[17] First, because of enthalpic factors, from silanol groups on the silica/zeolite spheres to bridge the polymer chains through hydrogen bonding. Second, due to entropic factors favoring the interpenetration on the whiskered surface vs. contact on the featureless non whiskered surface.

Gas permeation and sorption results

Pure 6FDA-DAM Membrane. Annealing Temperature and Plasticization Pressure. The choice of the final drying/annealing temperature can stabilize a membrane against mild swelling-induced plasticization with some reduction in permeability by reducing excess free volume.[45,46] Duthie et al.[45] showed an increased CO_2 pressure at the onset of plasticization from 1500 kPa to 2200 kPa after annealing 6FDA-TMPDA at 250°C for 24 h, compared with standard drying (80°C for 15 h and later 48 h under vacuum at 150°C). In this work, effects on permeation were studied using two annealing temperatures (180°C and 270°C) for pure 6FDA-DAM. Comparison to results by Kim et al.[46] for 6FDA-DAM membranes treated at a temperature 15°C above the T_g and quickly cooling down is also included. Table 1 shows that annealing at lower temperatures provides higher O_2, N_2, and CO_2 permeabilities with moderate losses in CO_2/N_2 and O_2/N_2 permselectivities. Comparing 180°C vs. 270°C similar permeabilities were obtained with reductions of 3–10% in selectivity depending on the gas pairs, thus, the lower annealing temperature was used for all 6FDA-DAM-based membranes.

Sorption measurements at 35°C for O_2, N_2, CH_4, and CO_2 in the bare 6FDA-DAM polymer membrane are given in Figure 6a. Figure 6b presents the O_2, N_2, CO_2, and CH_4 permeabilities of the pure 6FDA-DAM membrane annealed at 180°C for feed pressures up to 3500 kPa (measured using the standard constant volume system at 35°C with a vacuum downstream). Typical of most glassy polymers, the permeability decreases with increasing pressure due to saturation of excess

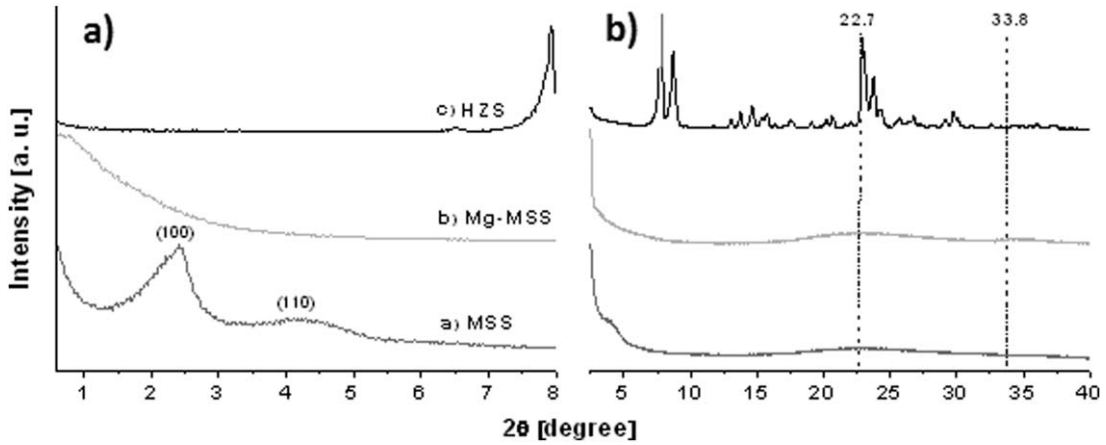

Figure 4. X-ray diffraction patterns of the powder materials: (a) MSSs, (b) Mg-MSSs, and (c) HZSs.

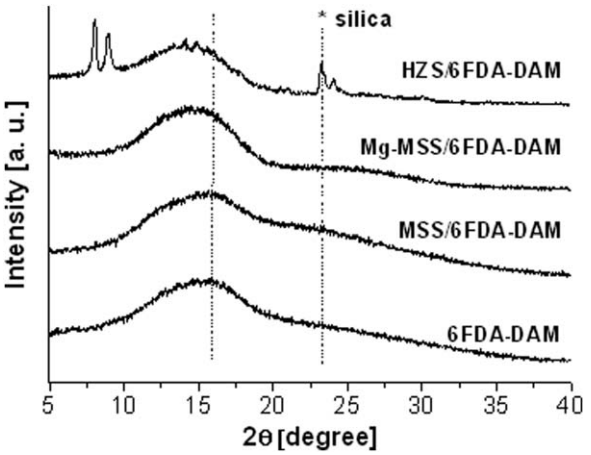

Figure 5. X-ray diffraction patterns of 6FDA-DAM membrane and MMMs based on 6FDA-DAM with 8 wt % loading of MSSs, Mg-MSSs, and HZSs.

unrelaxed volume in the glassy matrix for O_2, N_2, and CH_4 without an upward inflection. Conversely, after the initial drop in permeability for CO_2 between 1000 kPa and 2000 kPa, a minimum was reached at ~2000 kPa, similar to the reported by Damle et al.[47] (50°C). To avoid plasticization issues at 35°C conditions far from plasticization were used. Specifically a feed pressure with 200 kPa and permeate at vacuum was used for the constant volume system, while a feed pressure of 300 kPa with 100 kPa downstream was used for the Wicke–Kallenbach sweep gas method.

Single and Mixed-Gas Separation of MMMs-Based 6FDA-DAM. A comparison of membrane performance of MMMs fabricated at the same filler loading (8 wt %) of MSSs, Mg-MSSs, and HZSs are presented to illustrate properties of the three inorganic fillers (see Figure 7 and Table S1 in the Supporting Information). Increases in permeability and selectivity were obtained for all the MMMs compared to the pure polymer. The membranes based on the Grignard modified MSSs worked best with H_2/CH_4, CO_2/N_2, CO_2/CH_4, and O_2/N_2 separation selectivities of 21.8 (794 Barrer of H_2), 24.4 (1214 Barrer of CO_2), 31.5 (1245 Barrer of CO_2), and 4.3 (178 Barrer of O_2), respectively. This was probably due to a better contact between the polymer chain coils and the rougher whiskered MSS surfaces. In fact, Figure 7 indicates that CO_2 containing mixtures showed the largest selectivity increases, possibly reflecting favorable CO_2 interactions with the $Mg(OH)_2$ surface whisker-like structures. The CO_2/N_2 binary mixture selectivity increased from 18.8 to 24.4, and that for CO_2/CH_4 increased from 25.8 to 31.5 for MSSs and Mg-MSSs, respectively. Similarly, Shu et al.[34] showed higher CO_2/CH_4 selectivities, compared with non-modified zeolite 4A-based MMMs when using the same Grignard procedure, which exceeded the upper bound. These authors estimated whisker lengths of about 50 nm, similar to the hydrodynamic radii (32 nm) of the 6FDA-DAM coil diameter. They argued that the similarity of the polymeric chain dimensions and whisker dimensions may promote polymer coil accommodation in the environment somewhat close to its own configuration, which provides improved adsorption.

Table 1. O_2, N_2, and CO_2 Individual Permeability Values and O_2/N_2 and CO_2/N_2 Ideal Selectivities Corresponding to Plain 6FDA-DAM Membrane

Annealing T	180°C[a]	270°C[a]	T (°C)[b]
Gas			
P N_2 (Barrer)	39.1	20.2	17
P O_2 (Barrer)	131	74.3	55
P CO_2 (Barrer)	653	348	–
α O_2/N_2	3.3	3.6	3.3
α CO_2/N_2	16.7	17.2	–

[a]This work.
[b]Kim et al.[46] T (°C) = T_g+15; (T_g = 372°C).

The samples based on MSSs showed greater permeability increases vs. those based on HZSs. Conversely, the HZSs-based samples provided higher selectivities in comparison with MSSs (see also Table S1 Supporting Information). The same behavior was achieved when embedding these two fillers at 8 wt % loading in PSF and PI Matrimid® matrices.[35] The highest selectivity for H_2/CH_4 was 180 with a PH_2 of 38.4 Barrer for HZS/PI MMM, while PH_2 of 46.9 Barrer together with a H_2/CH_4 selectivity of 164 was found for MSS/PI MMM. PCO_2 of 12.6 Barrer (CO_2/N_2 selectivity 36.0) for MSS/PSF MMM, and CO_2/N_2 selectivity of 41.7 (PCO_2 of 7.2 Barrer) for HZS/PSF MMM were also found. Since both HZS and MSS particles are of approximately similar size, this improvement in selectivity for HZSs was attributed to the good bonding established between the external roughnesses of the hollow spheres composed of hundreds of silicalite-1 intergrown crystals.[35] Regarding MSSs, penetration of polymer segments into the mesoporosity of the filler may create a selective corona. Such an effect could produce higher selectivities for the hybrid system than expected for Knudsen diffusion in empty pores larger than the kinetic diameter of the gases of interest. Indeed, interactions between the dense polymer matrix and the sieves in the hybrid membrane may provide selective channels for gas separation processes.[14,16] Following such reasoning, Moaddeb et al.[48] reported that 6FDA-IPDA thin films formed on ceramic substrates whose pores had been impregnated with silica particles exhibited improved O_2/N_2 separation properties (selectivity of 9.3 vs. 5.3 of the pure polymer). This behavior was also found for other polymers such as 6FDA-MDA, 6FDA-6FpDA, 6FDA-6FmDA, PC, and TMHFPSF, providing better gas transport properties on the polymer films in the proximity of the silica particles.[48] In such cases, increases in O_2/N_2 selectivity and O_2 permeability were achieved beyond the upper bound limit for pure polymers.[2] The higher selectivities were attributed to increased rigidity of polymer matrix, with increases in the activation energy of diffusion due to adsorption of polymer to the surface of silica. Moreover, an increase in permeability resulted in disruption of polymer chain packing in the presence of the silica particles. Related reasoning was suggested for films containing ordered mesoporous silica and PSF to explain selective diffusivity, probably derived from hydrogen bonding with the OH-rich surface of the silica.[14,17]

Based on the above success, MMMs with 16 wt % were also prepared. Figure 8 shows the permeabilities and selectivities of the pure 6FDA-DAM membranes and MMMs containing 8 wt % and 16 wt % of MSSs in 6FDA-DAM. The constant volume method was used for CO_2, N_2, CH_4, and O_2 single gases, and the Wicke–Kallenbach method was used for H_2, CO_2, N_2, CH_4, and O_2 single gases and 50/50 vol % H_2/CH_4, CO_2/N_2, CO_2/CH_4, and O_2/N_2 binary mixtures. Typically a minimum of 2–3 different membranes were tested for each separation, and the average values (see Table S2 in the Supporting Information) gave standard deviation of the gas

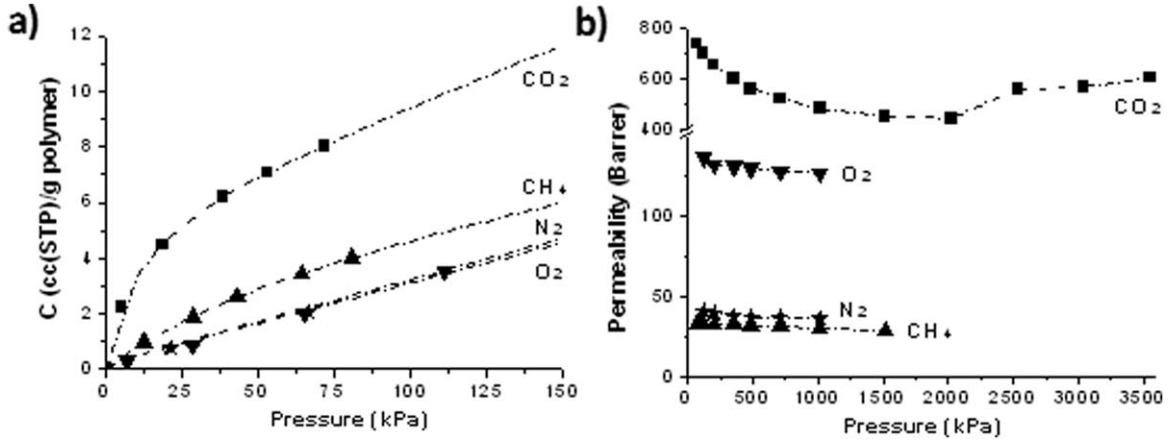

Figure 6. Sorbed gas concentration (a) and permeability (b) values as a function of absolute pressure for pure 6FDA-DAM membranes annealed at 180°C and tested at 35°C for O_2, N_2, CO_2, and CH_4 gases.

Dashed lines are to guide the eyes.

permeation measurements less than 5–10%. In general, the increased loading from 8 wt % to 16 wt % provided a large increase in permeability (producing in some cases even a rise of twofold) together with a significant increase in selectivity, as can be seen in detail in Supporting Information Table S2.

Pure gas transport often overestimate separation performance compared to the actual mixture cases due to various non-ideal sorption and transport phenomena with highly sorbing feeds.[49] In our case, however, measurements of single gas pairs and binary mixtures with the same Wicke–Kallenbach method showed minor differences in permeability and selectivity, and mixed gas permeabilities even gave more favorable selectivities in feeds containing carbon dioxide. Some successful CO_2 competitive sorption may be responsible for this effect. For 16 wt % MSS/6FDA-DAM MMM the CO_2/N_2 mixed gas selectivity rose from 20.0 for pure gas feed to 23.7

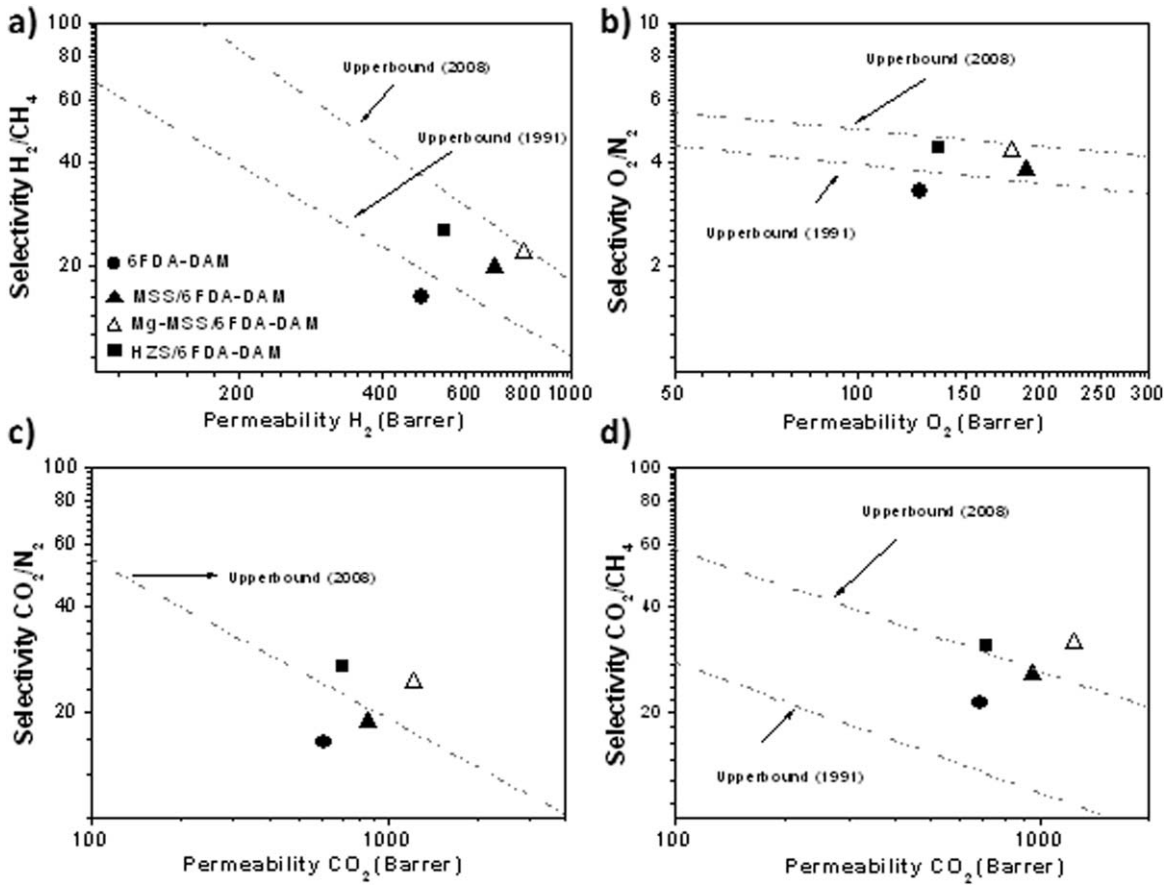

Figure 7. Mixed gas permeabilities and selectivities of pure 6FDA-DAM and 8 wt % filler (MSS, Mg-MSS, or HZS)/ 6FDA-DAM MMMs tested by Wicke–Kallenbach method for the binary mixtures (50/50 vol %): (a) H2/CH4, (b) O2/N2, (c) CO2/N2, and (d) CO2/CH4.

Measurements done at 35°C and ΔP of 200 kPa.

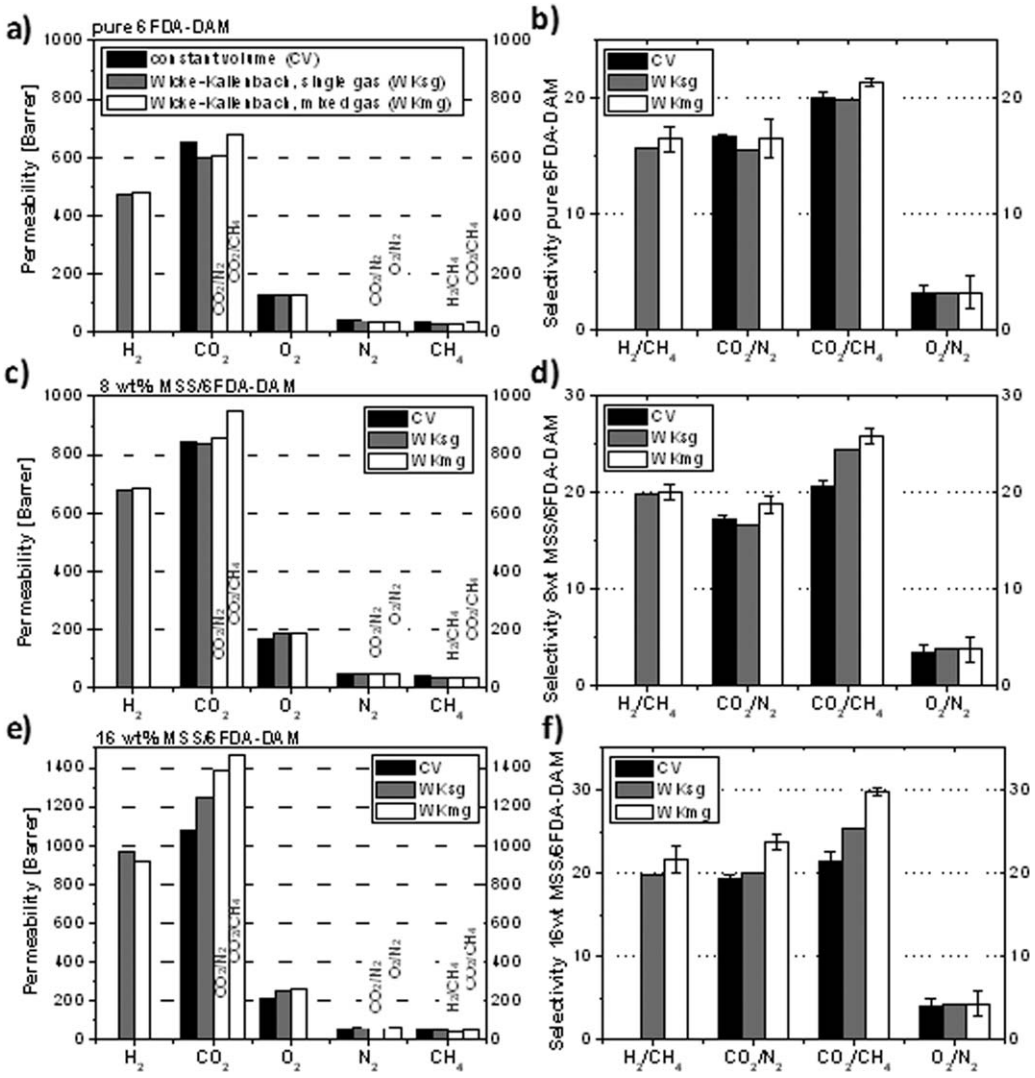

Figure 8. Permeabilities and selectivities for (a,b) pure 6FDA-DAM membrane, (c,d) 8 wt % MSS/6FDA-DAM MMMs, and (e,f) 16 wt % MSS/6FDA-DAM MMMs.

Constant volume method (CV) used for CO_2, N_2, CH_4, and O_2 single gases. The Wicke–Kallenbach method was used for H_2, CO_2, N_2, CH_4, and O_2 single gases (WKsg) and for 50/50 vol % H_2/CH_4, CO_2/N_2, CO_2/CH_4, and O_2/N_2 mixed gases (WKmg). Measurements done at 35°C and ΔP of 200 kPa.

in the 50% binary mixture. In the other separation containing carbon dioxide, CO_2/CH_4, selectivity also increased from 25.4 to 29.7 for the same membrane loading. Nevertheless, H_2/CH_4 selectivities are very similar for single and mixed gases, from 19.8 to 21.7, as well as for O_2/N_2, which has values from 4.1 to 4.3.

Conclusions

Efficient MMMs based on MSSs and the 6FDA-DAM polymer were observed for H_2, O_2, N_2, CO_2, and CH_4 single gas permeation. Good consistency was found using the constant volume or the Wicke–Kallenbach sweep gas approach. Permeabilities and selectivities from 50/50 vol % feed mixture measured for the H_2/CH_4, CO_2/N_2, CO_2/CH_4, and O_2/N_2 binary systems showed performance improvements being more relevant in the case of CO_2 containing mixtures when compared with single gas experiments. Transport analysis showed the post-casting annealing at 180°C produced good quality films. A study of permeability as a function of pressure indicated a CO_2 plasticization pressure at 2000 kPa for the pure polymer at 35°C.

Enhancement of the gas separation performance over the pure polymer was found with all filler membranes, surpassing the Robeson's upper bound for a fixed loading of 8 wt %. Mg-MSS-based membranes revealed the best performance linked to an improved interfacial filler-polymer contact with the 6FDA-DAM polymer due to the $Mg(OH)_2$ nanostructure modification, also evidenced by SEM-EDX, TGA, XRD, and N_2 adsorption. Excellent adhesion was also found for HZS MMMs by TEM due to its continuous shell of silicalite-1 crystals. Evidence for altered segmental spacing (by XRD) for the 6FDA-DAM polymer chains suggested the possibility of hindered segmental motion in the region near the particle surface of the MSSs. In addition, rising the MSSs loading from 8 wt % to 16 wt % nearly doubled apparent permeability with a considerable rise in selectivity. Still higher loadings of Mg-MSSs and HZSs in the 6FDA-DAM polymer matrix may be expected. In general MMMs prepared from 6FDA-DAM offered excellent permeabilities while those made of polymers

vastly used such as polysulfone or polyimide presented slightly higher selectivities, so MMMs offer opportunities to tailor gas membrane properties beyond those of pure polymers.

Acknowledgments

Financial support from the Spanish MINECO (MAT2013-40566-R), the Aragón Government and the ESF is gratefully acknowledged. B. Z. also thanks the funding from Fundación Ibercaja. Finally, the use of the Servicio General de Apoyo a la Investigación-SAI (Universidad de Zaragoza) is acknowledged.

Literature Cited

1. Chung TS, Jiang LY, Li Y, Kulprathipanja S. Mixed matrix membranes (MMMs) comprising organic polymers with dispersed inorganic fillers for gas separation. *Prog Polym Sci*. 2007;32(4):483–507.
2. Robeson LM. Correlation of separation factor versus permeability for polymeric membranes. *J Membr Sci*. 1991;62(2):165–185.
3. Robeson LM. The upper bound revisited. *J Membr Sci*. 2008; 320(1–2):390–400.
4. Powell CE, Qiao GG. Polymeric CO_2/N_2 gas separation membranes for the capture of carbon dioxide from power plant flue gases. *J Membr Sci*. 2006;279(1–2):1–49.
5. Merkel TC, Freeman BD, Spontak RJ, He Z, Pinnau I, Meakin P, Hill AJ. Ultrapermeable, reverse-selective nanocomposite membranes. *Science*. 2002;296(5567):519–522.
6. Tanh Jeazet HB, Staudt C, Janiak C. Metal-organic frameworks in mixed-matrix membranes for gas separation. *Dalton Trans*. 2012; 41(46):14003–14027.
7. Wind JD, Paul DR, Koros WJ. Natural gas permeation in polyimide membranes. *J Membr Sci*. 2004;228(2):227–236.
8. Qiu W, Chen C-C, Kincer MR, Koros WJ. Thermal analysis and its application in evaluation of fluorinated polyimide membranes for gas separation. *Polymer*. 2011;52(18):4073–4082.
9. Bos A, Punt IGM, Wessling M, Strathmann H. Plasticization-resistant glassy polyimide membranes for CO_2/CO_4 separations. *Sep. Purif Technol*. 1998;14(1–3):27–39.
10. Mikawa M, Nagaoka S, Kawakami H. Gas permeation stability of asymmetric polyimide membrane with thin skin layer: effect of molecular weight of polyimide. *J Membr Sci*. 2002;208(1–2):405–414.
11. Wind JD, Staudt-Bickel C, Paul DR, Koros WJ. The effects of crosslinking chemistry on CO_2 plasticization of polyimide gas separation membranes. *Ind Eng Chem Res*. 2002;41(24):6139–6148.
12. Qiu W, Xu L, Chen C-C, Paul DR, Koros WJ. Gas separation performance of 6FDA-based polyimides with different chemical structures. *Polymer*. 2013;54(22):6226–6235.
13. Zhang C, Dai Y, Johnson JR, Karvan O, Koros WJ. High performance ZIF-8/6FDA-DAM mixed matrix membrane for propylene/propane separations. *J Membr Sci*. 2012;389:34–42.
14. Reid BD, Ruiz-Trevino A, Musselman IH, Balkus KJ, Ferraris JP. Gas permeability properties of polysulfone membranes containing the mesoporous molecular sieve MCM-41. *Chem Mater*. 2001;13(7): 2366–2373.
15. Kim S, Marand E, Ida J, Guliants VV. Polysulfone and mesoporous molecular sieve MCM-48 mixed matrix membranes for gas separation. *Chem Mater* 2006;18(5):1149–1155.
16. Kim S, Marand E. High permeability nano-composite membranes based on mesoporous MCM-41 nanoparticles in a polysulfone matrix. *Microporous Mesoporous Mater*. 2008;114(1–3):129–136.
17. Zornoza B, Irusta S, Tellez C, Coronas J. Mesoporous silica sphere-polysulfone mixed matrix membranes for gas separation. *Langmuir*. 2009;25(10):5903–5909.
18. Zornoza B, Tellez C, Coronas J. Mixed matrix membranes comprising glassy polymers and dispersed mesoporous silica spheres for gas separation. *J Membr Sci*. 2011;368(1–2):100–109.
19. Ahn J, Chung W-J, Pinnau I, Guiver MD. Polysulfone/silica nanoparticle mixed-matrix membranes for gas separation. *J Membr Sci*. 2008;314(1–2):123–133.
20. Vu DQ, Koros WJ, Miller SJ. Mixed matrix membranes using carbon molecular sieves - I. Preparation and experimental results. *J Membr Sci*. 2003;211(2):311–334.
21. Kim S, Chen L, Johnson JK, Marand E. Polysulfone and functionalized carbon nanotube mixed matrix membranes for gas separation: theory and experiment. *J Membr Sci*. 2007;294(1–2):147–158.
22. Zornoza B, Gorgojo P, Casado C, Téllez C, Coronas J. Mixed matrix membranes for gas separation with special nanoporous fillers. *Desalalination Water Treat*. 2011;27(1–3):42–47.
23. Shu S, Husain S, Koros WJ. Formation of nanostructured zeolite particle surfaces via a Halide/Grignard route. *Chem Mater*. 2007; 19(16):4000–4006.
24. Liu JQ, Bae TH, Qiu WL, Husain S, Nair S, Jones CW, Chance RR, Koros WJ. Butane isomer transport properties of 6FDA-DAM and MFI-6FDA-DAM mixed matrix membranes. *J Membr Sci*. 2009; 343(1–2):157–163.
25. Bae TH, Lee JS, Qiu W, Koros WJ, Jones CW, Nair S. A high-performance gas-separation membrane containing submicrometer-sized metal-organic framework crystals. *Angew Chem Int Ed*. 2010; 49(51):9863–9866.
26. Zornoza B, Martinez-Joaristi A, Serra-Crespo P, Tellez C, Coronas J, Gascon J, Kapteijn F. Functionalized flexible MOFs as fillers in mixed matrix membranes for highly selective separation of CO(2) from CH(4) at elevated pressures. *Chem Commun*. 2011;47(33): 9522–9524.
27. Goh PS, Ismail AF, Sanip SM, Ng BC, Aziz M. Recent advances of inorganic fillers in mixed matrix membrane for gas separation. *Sep Purif Technol*. 2011;81(3):243–264.
28. Aroon MA, Ismail AF, Matsuura T, Montazer-Rahmati MM. Performance studies of mixed matrix membranes for gas separation: a review. *Sep. Purif Technol*. 2010;75(3):229–242.
29. Zornoza B, Tellez C, Coronas J, Gascon J, Kapteijn F. Metal organic framework based mixed matrix membranes: an increasingly important field of research with a large application potential. *Microporous Mesoporous Mater*. 2013;166:67–78.
30. Moore TT, Koros WJ. Non-ideal effects in organic-inorganic materials for gas separation membranes. *J Mol Struct*. 2005;739(1–3): 87–98.
31. Koros WJ, Mahajan R. Pushing the limits on possibilities for large scale gas separation: which strategies? *J Membr Sci*. 2000;175(2): 181–196.
32. Kresge CT, Leonowicz ME, Roth WJ, Vartuli JC, Beck JS. Ordered mesoporous molecular-sieves synthesized by a liquid-crystal template mechanism. *Nature*. 1992;359(6397):710–712.
33. Khan AL, Klaysom C, Gahlaut A, Vankelecom IFJ. Polysulfone acrylate membranes containing functionalized mesoporous MCM-41 for CO2 separation. *J Membr Sci*. 2013;436:145–153.
34. Shu S, Husain S, Koros WJ. A general strategy for adhesion enhancement in polymeric composites by formation of nanostructured particle surfaces. *J Phys Chem C*. 2007;111(2):652–657.
35. Zornoza B, Esekhile O, Koros WJ, Téllez C, Coronas J. Hollow silicalite-1 sphere-polymer mixed matrix membranes for gas separation. *Sep Purif Technol*. 2011;77(1):137–145.
36. Schulz-Ekloff G, Rathousky J, Zukal A. Mesoporous silica with controlled porous structure and regular morphology. *Int J Inorg Mater*. 1999;1(1):97–102.
37. Navascues N, Tellez C, Coronas J. Synthesis and adsorption properties of hollow silicalite-1 spheres. *Microporous Mesoporous Mater*. 2008;112(1–3):561–572.
38. Bae T-H, Liu J, Thompson JA, Koros WJ, Jones CW, Nair S. Solvothermal deposition and characterization of magnesium hydroxide nanostructures on zeolite crystals. *Microporous Mesoporous Mater*. 2011;139(1–3):120–129.
39. Vora RH. Process of making a shaped article from intermediate molecular weight polyimide. US Patent 4,933,132, 1990.
40. Koros WJ, Paul DR, Rocha AA. Carbon dioxide sorption and transport in polycarbonate. *J Polym Sci A Polym Phys*. 1976;14(4):687–702.
41. Moore TT, Damle S, Williams PJ, Koros WJ. Characterization of low permeability gas separation membranes and barrier materials; design and operation considerations. *J Membr Sci*. 2004;245(1–2): 227–231.
42. Ruthven D. *Principles of Adsorption and Adsorption Processes*. New York: Wiley, 1984:464.
43. Husain S, Koros WJ. Mixed matrix hollow fiber membranes made with modified HSSZ-13 zeolite in polyetherimide polymer matrix for gas separation. *J Membr Sci*. 2007;288(1–2):195–207.

44. Barton TJ, Bull LM, Klemperer WG, Loy DA, McEnaney B, Misono M, Monson PA, Pez G, Scherer GW, Vartuli JC, Yaghi OM. Tailored porous materials. *Chem Mater*. 1999;11(10):2633–2656.
45. Duthie X, Kentish S, Pas SJ, Hill AJ, Powell C, Nagai K, Stevens G, Qiao G. Thermal treatment of dense polyimide membranes. *J Polym Sci B*. 2008;46(18):1879–1890.
46. Kim JH, Koros WJ, Paul DR. Physical aging of thin 6FDA-based polyimide membranes containing carboxyl acid groups. Part I. Transport properties. *Polymer*. 2006;47(9):3094–3103.
47. Damle S, Koros WJ. Permeation equipment for high-pressure gas separation membranes. *Ind Eng Chem Res*. 2003;42(25):6389–6395.
48. Moaddeb M, Koros WJ. Gas transport properties of thin polymeric membranes in the presence of silicon dioxide particles. *J Membr Sci*. 1997;125(1):143–163.
49. Esekhile O, Qiu W, Koros WJ. Permeation of butane isomers through 6FDA-DAM dense films. *J Polym Sci B Polym Phys*. 2011;49(22):1605–1620.

Manuscript received May 8, 2015, and revision received June 24, 2015.